Scientia Iranica B (2023) 30(6), 1955–1972

Sharif University of Technology
Scientia Iranica
Transactions B: Mechanical Engineering
http://scientiairanica.sharif.edu

Investigating the effect of noise and solution order on calculating the impedance of electrochemical systems using impedance spectroscopy in the time domain

R. Hamedi[a,*], F. Torabi[a], and J.B. Ghasemi[b]

a. *Mechanical Engineering Faculty, K.N. Toosi University of Technology, Tehran, Iran.*
b. *Department of Analytical Chemistry , Chemistry Faculty, School of Sciences, University of Tehran, Tehran, Iran.*

Received 4 April 2022; received in revised form 4 November 2022; accepted 21 February 2023

KEYWORDS
Fast Fourier Transform;
Impedance;
Numerical fourier transform;
Solution order;
Noise.

Abstract. Fast Fourier Transform (FFT) is a standard method for calculating the numerical Fourier transform as well as the impedance of electrochemical systems. However, the presence of noise in data increases the error rate while calculating the numerical Fourier transform and in order to reduce the error rate in noisy conditions, the solution order of the Fourier transform should be enhanced. In the present study, the solution order used for calculating the numerical Fourier transform in the presence of noise was enhanced using a straight line and then second- and third-order polynomials. Next, the impedance of the series, parallel, and battery circuits was calculated. Additionally, the calculated impedance of the higher-order solutions was compared to the acquired impedance through the FFT method in noisy conditions. The findings of this study demonstrated that increasing the solution order of the numerical Fourier transform from zero up to one would yield satisfactory results; however, further enhancement would deteriorate the outcome responses. Therefore, it can be concluded that the linear method is the best way for calculating the numerical Fourier transform in the presence of noise.

1. Introduction

Electrochemical Impedance Spectroscopy (EIS) is one of the most powerful methods for characterization of electrochemical systems such as batteries and fuel cells. In this method, the electrochemical system is stimulated by a voltage or current sinusoidal input signal. Then, the system response that is either a voltage or current response (according to the input) is measured. Finally, the impedance, i.e., division of voltage in the frequency domain into current in the frequency domain, is calculated. This procedure is repeated for a wide range of frequencies (from microhertz to megahertz) which makes EIS a time-consuming procedure. Of note, the EIS technique requires low disturbances and steady-state conditions, hence the need for costly devices. Despite these drawbacks, many researchers still use this technique to evaluate the behavior of electrochemical systems. Janicka et al. [1] used EIS to study the variations in the fuel cell impedance in a wide range of current loads and humidity changes. These changes in the impedance determined the variant processes occurring in the fuel

*. *Corresponding author.*
E-mail addresses: r.hamedi@email.kntu.ac.ir (R. Hamedi); ftorabi@kntu.ac.ir (F. Torabi); jahan.ghasemi@ut.ac.ir (J.B. Ghasemi)

doi: 10.24200/sci.2023.60214.6668

cell. Qiu et al. [2] studied the initial discharge/charge process in the Li-S batteries with different potentials using the EIS. They also characterized the electronic and ionic transport properties of a sulfur electrode in a Li-S battery. Sharma et al. [3] used EIS to analyze the changes in equivalent circuit parameters of solar cells as well as their degradation degree. Xiao et al. [4] investigated the effect of State of Charge (SoC) on the parameters of an equivalent circuit model in Li-ion batteries using the EIS. Gallo et al. [5] employed the EIS method to estimate Solid Oxide Fuel Cell (SOFC) voltage degradation over time along with its nominal behavior. Erts et al. [6] utilized EIS as an effective tool for determining the oxidation level of Bi2Se3 surfaces, quality of the surface covering, and characterization of the type and parameters of the nanopores in Bi2Se3 thin films. Calles et al. [7] studied Prismatic Li-ion cells with the nominal capacity of 25 Ah (as used for automotive applications) with EIS. They reported the interdependency of the parameters determined by the EIS for cells in different aging regimes (cyclic vsersus non-cyclic aging) relevant to automotive requirements use cases. Gopalakrishnan et al. [8] characterized the Nickel Manganese Cobalt (NMC) Li-ion batteries and determined the contribution of temperature and SoC to the EIS. Li et al. [9] proposed two models for SoC and State of Health (SoH) estimation based on EIS. Koseoglou et al. [10] used the EIS for Li plating detection in Li-ion batteries during the charging procedure. Ezpeleta et al. [11] also utilized the EIS to characterize commercial cylindrical Li-ion cells under different SoC conditions up to 300 charge/discharge cycles to monitor the SoH status. Capkova et al. [12] investigated the electrochemical reactions in a 3.4 Ah Li-S pouch cell. Using EIS, they characterized electrode processes, complex interfaces, and internal resistance. Mohsin et al. [13] presented a new and original method to determine the SoH of the lead-acid battery from EIS. They also found a reliable formula to link the SoH and EIS with unknown battery history.

Another method employed to determine the electrochemical system impedance is the EIS method in the time domain. In this technique, the system is stimulated by a voltage or current input signal in the time domain. Afterwards, the system response that is either a current or voltage signal in the time domain (according to the input signal) is measured. Ultimately, the system impedance is calculated by dividing the voltage Fourier Transform (FT) by the current FT.

The time domain method is significantly more efficient than the frequency domain method mainly because the entire spectrum can be obtained from a single data set. In addition, instrumentation for the time domain method is simple and inexpensive. Lohman et al. [14] reported that the EIS method requires more time than the EIS in the time domain. In another study, Klotz [15] concluded that the EIS in the time domain decreased the required time needed for performing the EIS method by 71.2%.

A number of researchers have considered application of EIS in the time domain to determine the behavior of electrochemical systems. Gantenbein et al. [16] presented a Li-ion cell model that functioned based on physically meaningful equivalent circuit model parameterized by EIS in the time domain. Jiang et al. [17] developed a portable EIS system in the time domain that performed Fast Fourier Transform (FFT) to calculate impedance in bio-detection. Lyu et al. [18] used the EIS in the time domain to characterize the electrochemical electrodes and estimate the SoH of Lithium Cobalt Oxide ($LiCoO_2$) Li-ion batterie. Lyu et al. [19] used EIS in the time domain to obtain the impedance of Li-ion batteries and compared it with the conventional EIS method. They concluded that compared with standard the EIS, the time domain measurement greatly reduced the acquisition time. Zappen et al. [20] applied EIS in the time domain to acquire the impedance spectra during the charging process of a Li-ion battery with high time resolution. Kuzniestov et al. [21] used EIS in the time domain and applied it to a battery management system in an electric vehicle. De Angelis et al. [22] used EIS in the time domain to characterize the 18650 Li-ion battery. Fu et al. [23] employed EIS in the time domain to estimate the SoH of the Li-ion battery. They proposed a fast impedance calculation-based battery SoH estimation method for Li-ion batteries from the perspective of EIS in the time domain.

Since discrete data in the EIS method in the time domain represent the voltage and current, their FTs must be calculated numerically. The standard numerical method for the FT calculation on a series of discrete data is FFT. It will be elaborated later in this study that this method is a single-point estimation method with zero- order accuracy. In the absence of noise, the FFT method has quite low error, meaning that it is fairly suitable for EIS calculation. However, a high error rate is observed during the calculation of electrochemical system impedance in noisy conditions [24,25]. Klotz et al. [26] proposed a linear method for EIS in the time domain. In this method, the numerical FT is calculated using two subsequent time-point data. This technique enhances the solution order and yields more appropriate solutions in noisy conditions. Therefore, it seems that increasing the solution order of the FT will reduce the calculation error of the electrochemical system impedance in the presence of noise.

In the present study, the FFT (zero-order) was compared with one-, two-, and three-order polynomial

approximations to find out the more robust one in the presence of noise. To this end, the EIS in the time domain is calculated using a straight line as well as the second- and third-order polynomials for series, parallel, and battery circuits in noisy conditions. Finally, the results were compared with the calculated impedances obtained from the FFT method. In other words, the effect of increasing the solution order on the numerical FT calculation in the presence of noise was investigated. The structure of the present research is organized in three sections as follows:

(i) This section presents the method for the solution order enhancement in the numerical FT calculation;

(ii) This section makes a comparison between the higher-order solution methods with its FFT counterpart in series, parallel, and battery circuits;

(iii) This section gives the concluding remarks.

2. Increasing the solution order in the numerical FT calculation

The FT of the arbitrary function of $f(t)$ is equal to $f(\omega)$, which is calculated based on Eq. (1):

$$f(\omega) = \int_{-\infty}^{+\infty} f(t)exp(-j\omega t)dt, \tag{1}$$

where ω indicates the frequency, t specifies the time, and j represents the imaginary unit.

Since both voltage and current are given as discrete data, the numerical FT must be used to transform both voltage and current from the time domain into the frequency domain according to Eq. (2). In this equation, F_k indicates the FT of the f function at the frequency number of k, N the number of points, i the counter of points, and f_i the value of the f function at the ith point.

$$F_k = \sum_{i=0}^{N-1} f_i exp\left(-j\left(\frac{2\pi i}{N}\right)k\right) \qquad k = 0, ..., N-1. \tag{2}$$

As shown in Eq. (1), the FT of $f(t)$ is used to transfer the function $f(t)$ from the time domain into the frequency domain, meaning that the output of Eq. (1) is a function of frequency. Since the obtained data from the experimental tests or simulations are discrete, the integral in Eq. (1) is converted into Eq. (2), and this relation is further used for all of the calculations in the present paper. In this equation, the parameter k indicates the frequency number, and the frequency value equals $\left(\frac{2\pi i}{N}\right)k$. Here, the frequency for different values of k is obtained through the following numerical sequence:

$$\begin{cases} k = 1 \rightarrow \omega = 0, \frac{2\pi}{N}, \frac{2\pi}{N} \\ \qquad \times 2, ..., \frac{2\pi}{N} \times (n-1) \\ k = 2 \rightarrow \omega = 0, \left(2 \times \frac{2\pi}{N}\right), \left(2 \times \frac{2\pi}{N}\right) \\ \qquad \times 2, ..., \left(2 \times \frac{2\pi}{N}\right) \times (n-1) \\ k = 3 \rightarrow \omega = 0, \left(3 \times \frac{2\pi}{N}\right), \left(3 \times \frac{2\pi}{N}\right) \\ \qquad \times 2, ..., \left(3 \times \frac{2\pi}{N}\right) \times (n-1) \end{cases} \tag{3}$$

A comparison of Eqs. (1) and (2) reveals that FFT is quite similar to the numerical integration of Eq. (1) based on the midpoint rule. According to the fundamentals of the numerical methods, the midpoint rule is referred to as a zero-order method where a zero-order polynomial (a constant value) is replaced instead of the main function. This concept poses this question that what would happen if we increase the order of integrating polynomial? In other words, what would happen if we use the trapezoidal rule and the Simpson's rule or even we increase the order of integration even more? This section briefly explains how to increase the order of the integration.

According to Eq. (1), the FTs of $V(t)$ and $I(t)$ can be calculated through Eqs. (4) and (5), respectively:

$$V(\omega) = \int_{-\infty}^{+\infty} V(t)exp(-j\omega t)dt, \tag{4}$$

$$I(\omega) = \int_{-\infty}^{+\infty} I(t)exp(-j\omega t)dt. \tag{5}$$

Additionally, Euler's equation is according to Eq. (6):

$$exp(-j\omega t) = \cos(\omega t) - j\sin(\omega t). \tag{6}$$

By substituting Eq. (6) into Eq. (4) and assuming that the time variable is an a positive value, we can obtain Eq. (7) as:

$$V(\omega) = \int_0^{+\infty} V(t)\cos(\omega t)dt - j\int_0^{+\infty} V(t)\sin(\omega t)dt. \tag{7}$$

As observed, Eq. (7) includes a real and an imaginary part, which are defined according to Eqs. (8) and (9), respectively:

$$Re_V(\omega) = \int_0^{+\infty} V(t)\cos(\omega t)dt, \tag{8}$$

$$Im_V(\omega) = -\int_0^{+\infty} V(t)\sin(\omega t)dt. \tag{9}$$

By substituting Eqs. (8) and (9) into Eq. (7), Eq. (10) is obtained as:

$$V(\omega) = Re_V(\omega) + jIm_V(\omega). \tag{10}$$

Similar to these equations, the FT of the current is achieved through Eq. (11):

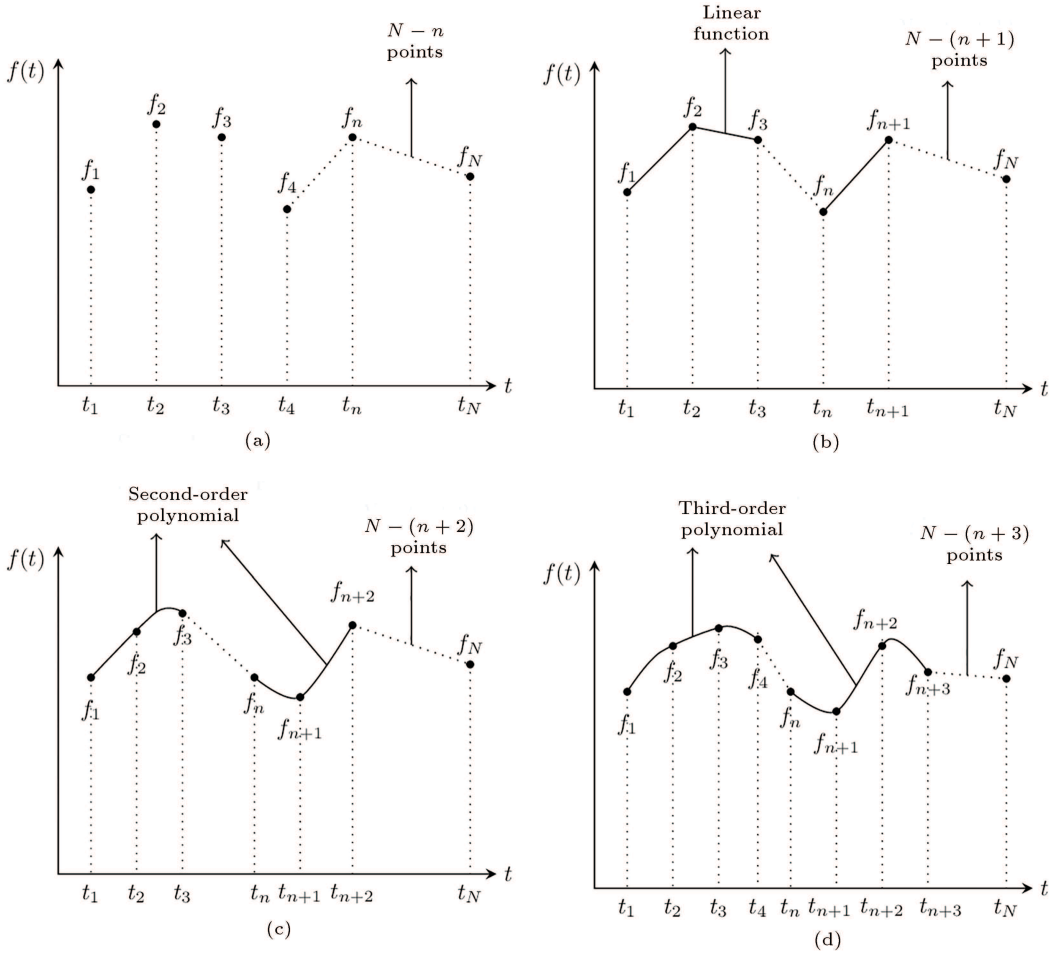

Figure 1. Description of the FFT, linear, and second- and third-order polynomial FT.

$$I(\omega) = Re_I(\omega) + jIm_I(\omega). \tag{11}$$

In the present paper, the $V(t)$ and $I(t)$ functions are considered mth-order polynomial functions using voltage and current data at every $m+1$ succeeding points according to Figure 1. As a result, Eqs. (8) and (9) are transformed into Eqs. (12) and (13), as shown below:

$$Re_V(\omega) = \sum_{n=0}^{N_g-1} \int_{t_{nm+1}}^{t_{(n+1)m+1}} (a_m t^m + a_{m-1}t^{m-1} + ... + a_0)\cos(\omega t)dt, \tag{12}$$

$$Im_V(\omega) = -\sum_{n=0}^{N_g-1} \int_{t_{nm+1}}^{t_{(n+1)m+1}} (a_m t^m + a_{m-1}t^{m-1} + ... + a_0)\sin(\omega t)dt. \tag{13}$$

In these equations, $(a_m t^m + a_{m-1}t^{m-1} + ... + a_0)$ is the mth-order polynomial of the voltage, and $a_0, \cdots, a_{m-1}, a_m$ are the constant coefficients of the polynomial of the voltage between the t_{nm+1} and $t_{(n+1)m+1}$ time points. To be specific, m indicates the degree of polynomial passes through $m+1$ consecutive points. Also, t_{nm+1} and $t_{(n+1)m+1}$ are the beginning and end points of each integral interval, respectively, and n is the counter of polynomials between this time interval. In addition, N_g is the number of mth-order polynomials in the time interval.

For each of $m+1$ successive points of $t_0, \cdots, t_{m-1}, t_m$, the corresponding voltages are $v_0, \cdots, v_{m-1}, v_m$, respectively. Therefore, upon including these $m+1$ points in the mth-order polynomial, a system of $m+1$ equations with $m+1$ unknown variables are formed according to the system of Eq. (14) based on which, the constant coefficients of $a_0, \cdots, a_{m-1}, a_m$ can be obtained:

$$\begin{cases} a_m {t_m}^m + a_{m-1}{t_m}^{m-1} + ... + a_0 = v_m \\ a_m {t_{m-1}}^m + a_{m-1}{t_{m-1}}^{m-1} + ... + a_0 = v_{m-1} \\ \vdots \\ a_m {t_0}^m + a_{m-1}{t_0}^{m-1} + ... + a_0 = v_0 \end{cases} \tag{14}$$

Therefore, the constant coefficients of $a_1, \cdots, a_{m-1}, a_m$ are initially calculated by system of Eq. (14). Then, these coefficients are substituted into Eqs. (12) and (13) and subsequently, they are applied to Eq. (10).

A similar process is performed to calculate the FT of current. Of note, the Z impedance is calculated according to Eq. (15):

$$Z(\omega) = \frac{V(\omega)}{I(\omega)}. \quad (15)$$

3. Validation of the proposed method by comparing it with the analytical method

Different shapes of input voltage were taken into account in the present study. As a sample, a step function is shown in Figure 2, indicating that a noisy input voltage is applied to series, parallel, and battery circuits through simulations in Scilab software. As shown, this function starts at zero and ends at 150 seconds. the mean magnitude of this step starts at zero and changes to 4.2 after 25 seconds. Then, the mean value of this function is switched to zero again after 125 seconds.

To obtain a real condition in these simulations, the noise behavior does not follow a predefined function (for example, Gaussian noise, white noise, etc.), and the generated noise is random in nature. For this reason, it is recommended that a strict noise generation method be employed. In other words, random numbers are generated by the computational software and then added to the desired function. Thus, the noise frequency equals the input function sampling frequency, and its magnitude equals the randomly generated numbers of the computational software.

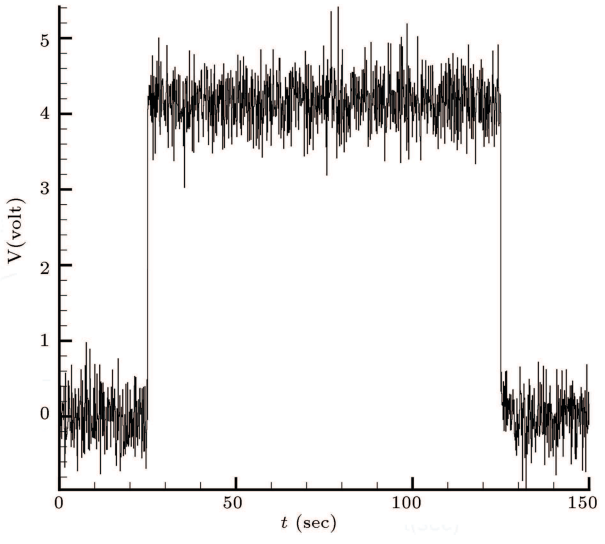

Figure 2. The noisy step pulse as the input signal.

The current is measured as output. Then, the FT of both voltage and current and impedance of the corresponding circuits are calculated using high-order FT and FFT. Finally, the Nyquist and bode diagrams of the impedance are plotted. The obtained results are finally investigated by comparing them with the analytical method and error calculation.

3.1. Series and parallel circuit

According to Figure 3(a), a series circuit is a circuit in which a capacitor and a resistor are connected in series to a voltage source. On the contrary, according to Figure 3(b), a parallel circuit is a circuit in which a capacitor and a resistor are connected in a parallel form that are also connected to a voltage source. In Figure 3(a) and (b), R and C are representatives of the ohmic resistance and capacitor capacity, respectively.

The values of the impedance, magnitude, and phase of the series and parallel circuits are obtained according to Table 1. In this table, Z_s and Z_p represent the series and parallel circuit impedance, respectively. Also, m_s, $Z_{s,re}$, and, $Z_{s,im}$ represent the magnitude value, real, and imaginary components of a series circuit impedance, respectively. Similarly, m_p, $Z_{p,re}$, and $Z_{p,im}$ indicate the magnitude value and real and imaginary parts of parallel, respectively. Moreover, θ_s and θ_p specify the impedance phase of the series and parallel circuits, respectively.

In the present paper, the output current was measured by performing simulations in Scilab software according to the instructions given in Figure 3(a) and (b) for different amounts of the capacitor and resistor and different forms of noisy input voltage. Furthermore, the impedance values of the series and parallel circuits were calculated using high-order FT and FFT. Despite the multiplicity of simulations performed in this study, all of them were not included in this report. Therefore, as a sample demonstration of these simulations, a noisy step input signal (according to Figure 2 and Table 2) is applied to the voltage source, and the output current is measured. In the next step, the FFT and high-order FT values of both voltage and current were calculated and then, the system

Table 1. The impedance, magnitude, and phase of the series and parallel circuits.

Circuit	Series	Parallel
Impedance	$Z_s = R + \frac{1}{jC\omega}$	$Z_p = \frac{R}{1+jRC\omega}$
Impedance magnitude	$m_s = \sqrt{{Z_{s,re}}^2 + {Z_{s,im}}^2}$	$m_p = \sqrt{{Z_{p,re}}^2 + {Z_{p,im}}^2}$
Impedance phase	$\theta_s = \arctan\left(\frac{Z_{s,im}}{Z_{s,re}}\right)$	$\theta_p = \arctan\left(\frac{Z_{p,im}}{Z_{p,re}}\right)$

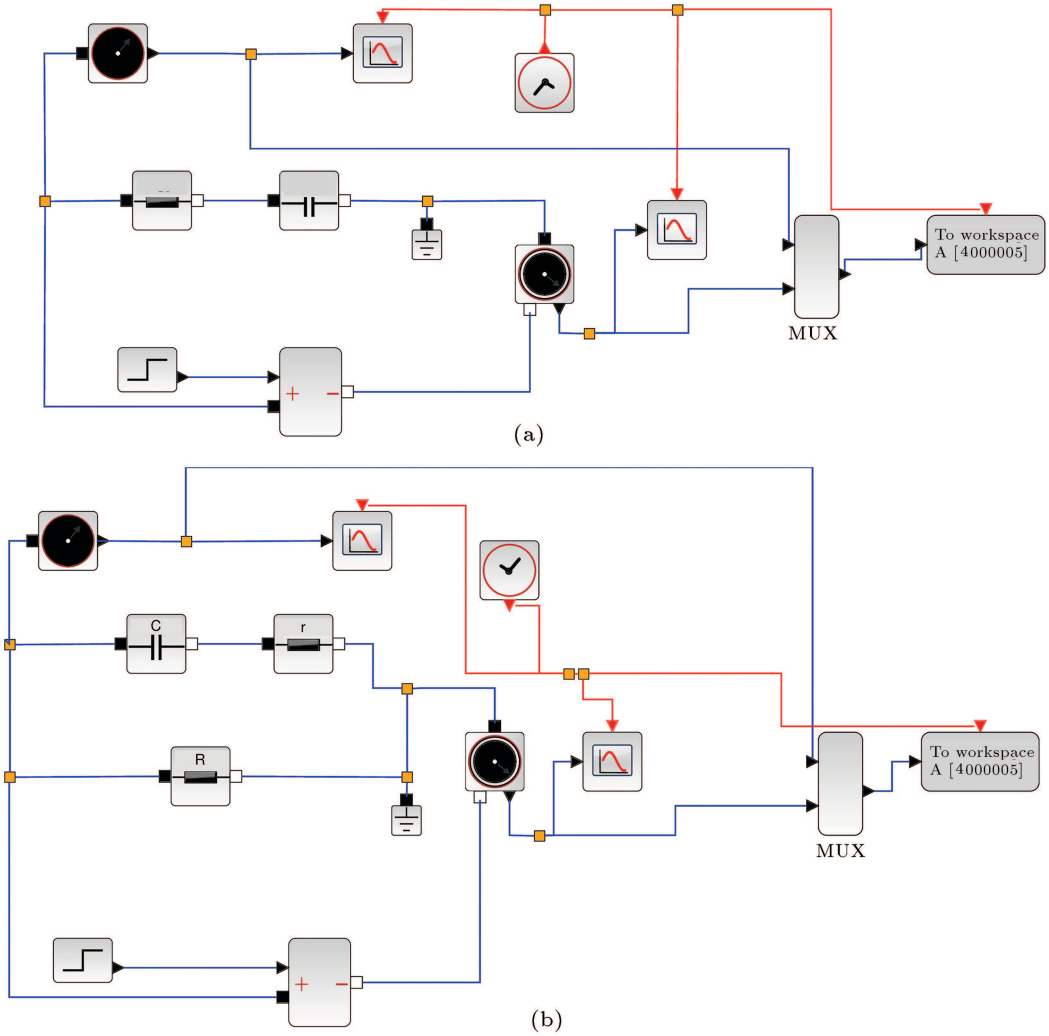

Figure 3. The series and parallel circuits in Scilab software.

Table 2. The condition of the sample test.

R (Ω)	C (F)	Time (s)	Time step (s)	V_s (v)
1000	0.001	150	0.001	Noisy step pulse (Figure 2)

impedance was measured by dividing the FT of voltage by the FT of current. Ultimately, the Nyquist diagram and bode plot of impedance was drawn.

The Nyquist diagram of the series circuit impedance calculated using the FFT, linear, second-order, and third-order polynomials methods are illustrated in Figure 4(a)–(d), respectively. In addition, the theoretical Nyquist diagram of the series and parallel circuits are depicted in Figure 5(a) and (b), respectively. In Figure 5(a), sharper oscillations can be observed in the analytical Nyquist diagram through the FFT method. However, linear and second-order polynomial methods are in great agreement with the analytical Nyquist diagram. Moreover, no significant discrepancy is observed between the linear and second-order polynomial methods. In fact, increasing the solution order from the linear to the second-order merely increased the calculations volume with no tangible difference in the responses. On the contrary, the third-order polynomial method has a high error rate and compared to the analytical Nyquist diagram, no appropriate response could be obtained.

The diagrams of the magnitude values of the series circuit impedance regarding the frequency (the bode plot) calculated by the FFT, linear, second-order, and third-order polynomials methods are illustrated in Figure 6(a)–(d), respectively. The impedance phase diagrams of the series circuit with respect to the frequency (the bode plot) calculated by the FFT, linear, second-order, and third-order polynomials methods are

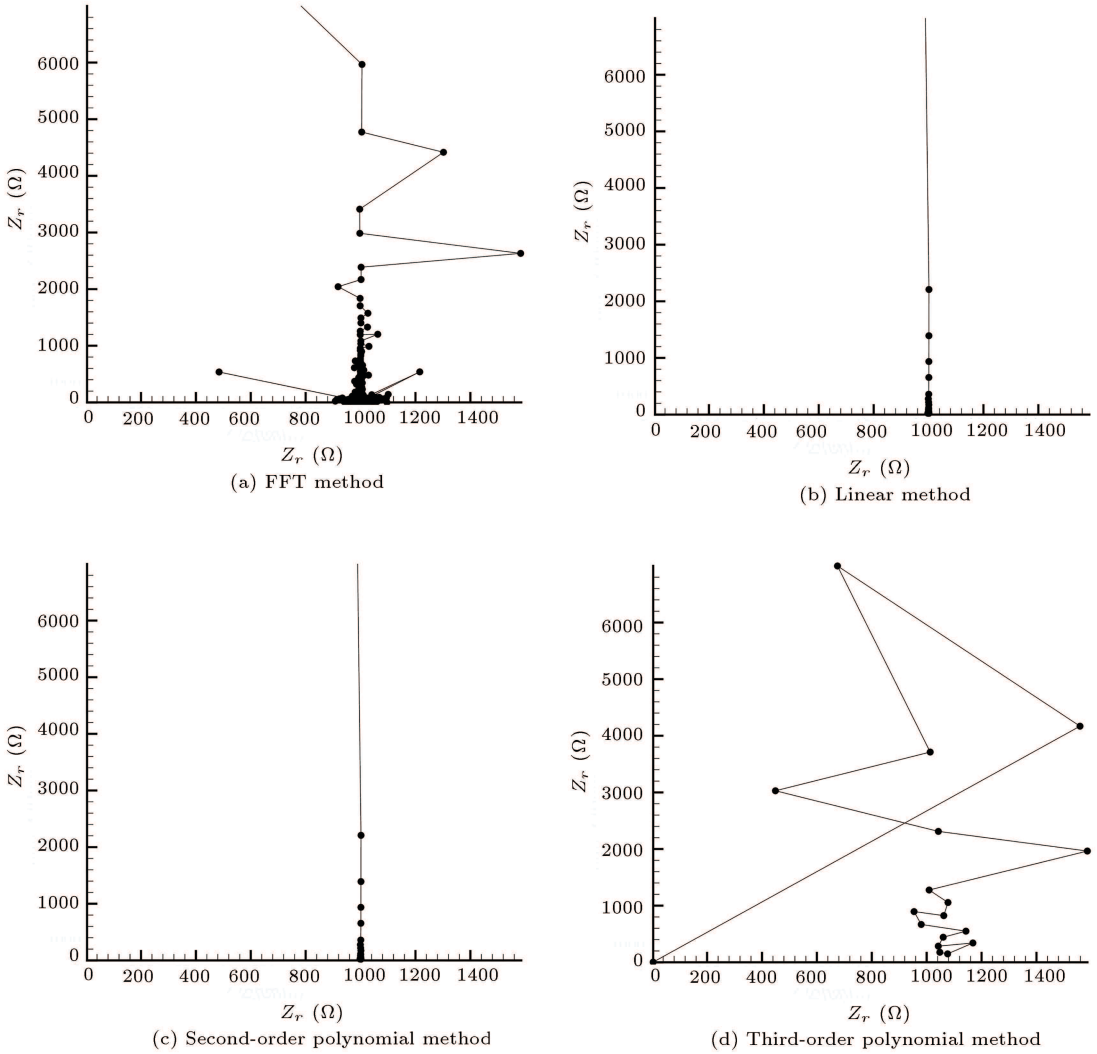

Figure 4. Impedance Nyquist plot of the series circuit in the condition described in Table 2.

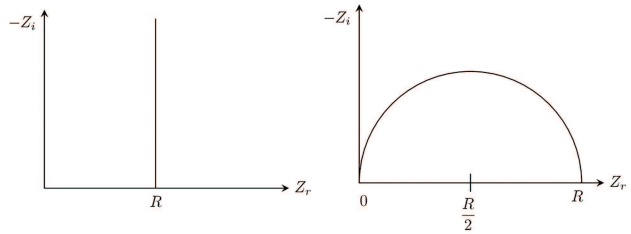

Figure 5. The impedance Nyquist plot of the series and parallel circuits.

depicted in Figure 7(a)–(d), respectively. As perceived, the results are as the same as those from the Nyquist diagrams of the series circuit.

In the present paper, a Complex Non-linear Least Square (CNLS) method was employed to calculate the error rate. CNLS is a method used to approximate a model by a linear one and refine its parameters through successive iterations. In this method, the appropriate model is recognized by minimizing Eq. (16) that represents the object function [27].

$$s = \sum_{i=1}^{N} w_i \left((Z_{re,i} - Z_{rea,i})^2 + (Z_{im,i} - Z_{ima,i})^2 \right), \quad (16)$$

where w_i is the inverse square of impedance magnitude. Moreover, $Z_{re,i}$ and $Z_{rea,i}$ respectively, represent the real parts of the measured and analytical impedance at the ith frequency. Additionally, $Z_{im,i}$ and $Z_{ima,i}$ indicate the imaginary part of measured and analytical impedance at the ith frequency, respectively. The above equation was used in this paper to measure the error rate of the impedance diagram. Lower values of this equation represent the lower error rate of the corresponding technique, and the lowest possible value of this equation is zero. Therefore, as this value decreases toward zero, the error rate decreases as well.

Another appropriateness criterion of the fitted impedance diagram in the CNLS method is given in Eqs. (17) and (18) [27]. In these equations, Δ_{re} and Δ_{im} denote the residual value of the real and imaginary parts of the impedance at the ith frequency, respec-

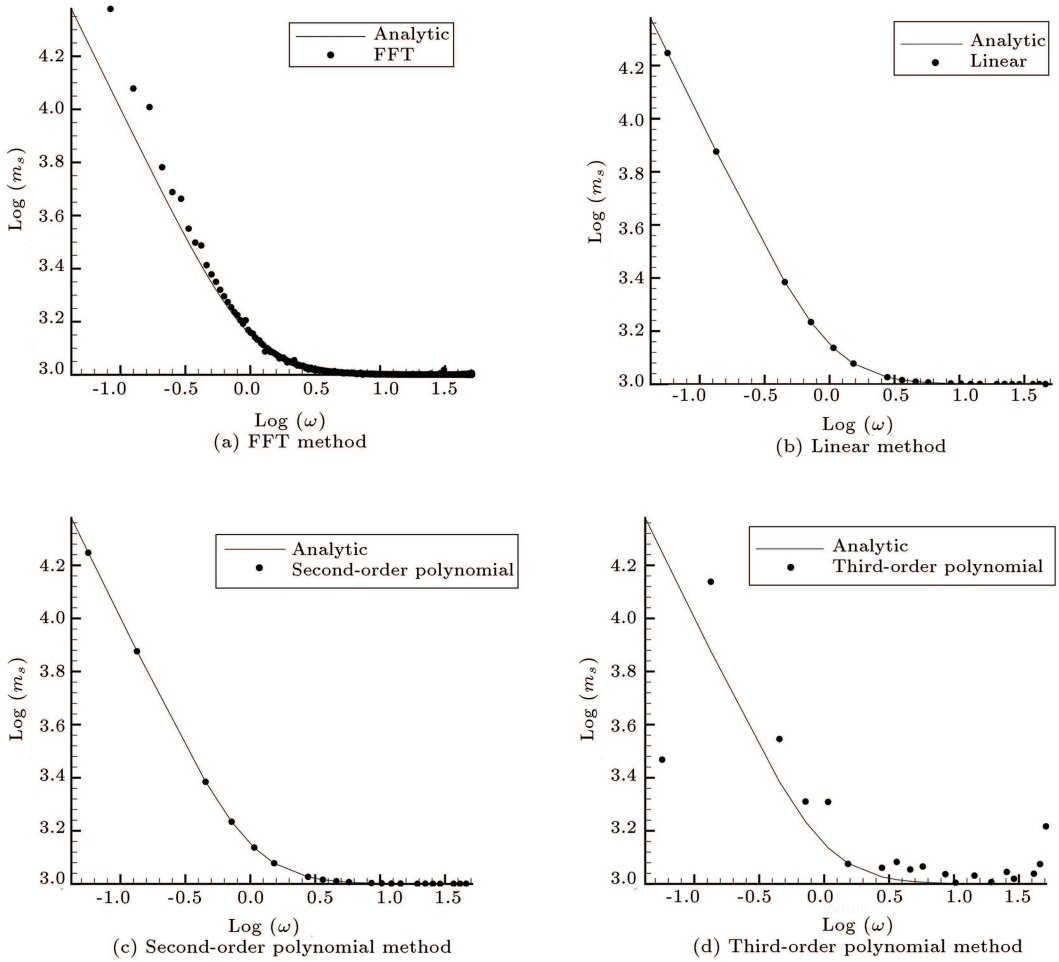

Figure 6. Impedance magnitude plot of the series circuit in the condition described in Table 2.

Table 3. The errors in the series circuit.

Error type	FFT	Linear	Second-order	Third-order
Δ_{re}	0.0198	0.0011	0.0020	0.1591
Δ_{im}	0.0031	9.0724×10^{-4}	0.0046	0.2303
s	46.6118	1.0855×10^{-4}	0.0075	4.3554×10^{6}

tively. In addition, $Z_{a,i}$ is the analytical impedance at the ith frequency.

$$\Delta_{re} = \sum_{i=1}^{N} \frac{Z_{re,i} - Z_{rea,i}}{|Z_{a,i}|}, \tag{17}$$

$$\Delta_{im} = \sum_{i=1}^{N} \frac{Z_{im,i} - Z_{ima,i}}{|Z_{a,i}|}. \tag{18}$$

The values of these equations vary at different frequencies. In the present paper, the average value of these equations was used for calculating the relative error. The mean values of Eqs. (17) and (18) was then calculated through Eqs. (19) and (20), respectively. In these equations, N is the number of the measured data. Similar to the previous paragraph, as the value of these equations decreases, their error rates decrease as well. Hence, it can be concluded that the corresponding method can be more appropriate than its counterparts.

$$\Delta_{re} = \frac{1}{N} \sum_{i=1}^{N} \left| \frac{Z_{re,i} - Z_{rea,i}}{|Z_{a,i}|} \right|, \tag{19}$$

$$\Delta_{im} = \frac{1}{N} \sum_{i=1}^{N} \left| \frac{Z_{im,i} - Z_{ima,i}}{|Z_{a,i}|} \right|. \tag{20}$$

The error rates of the simulated sample of the series circuit (according to Table 2 terms) are given in Table 3. Apparently, the error rates of the linear method are

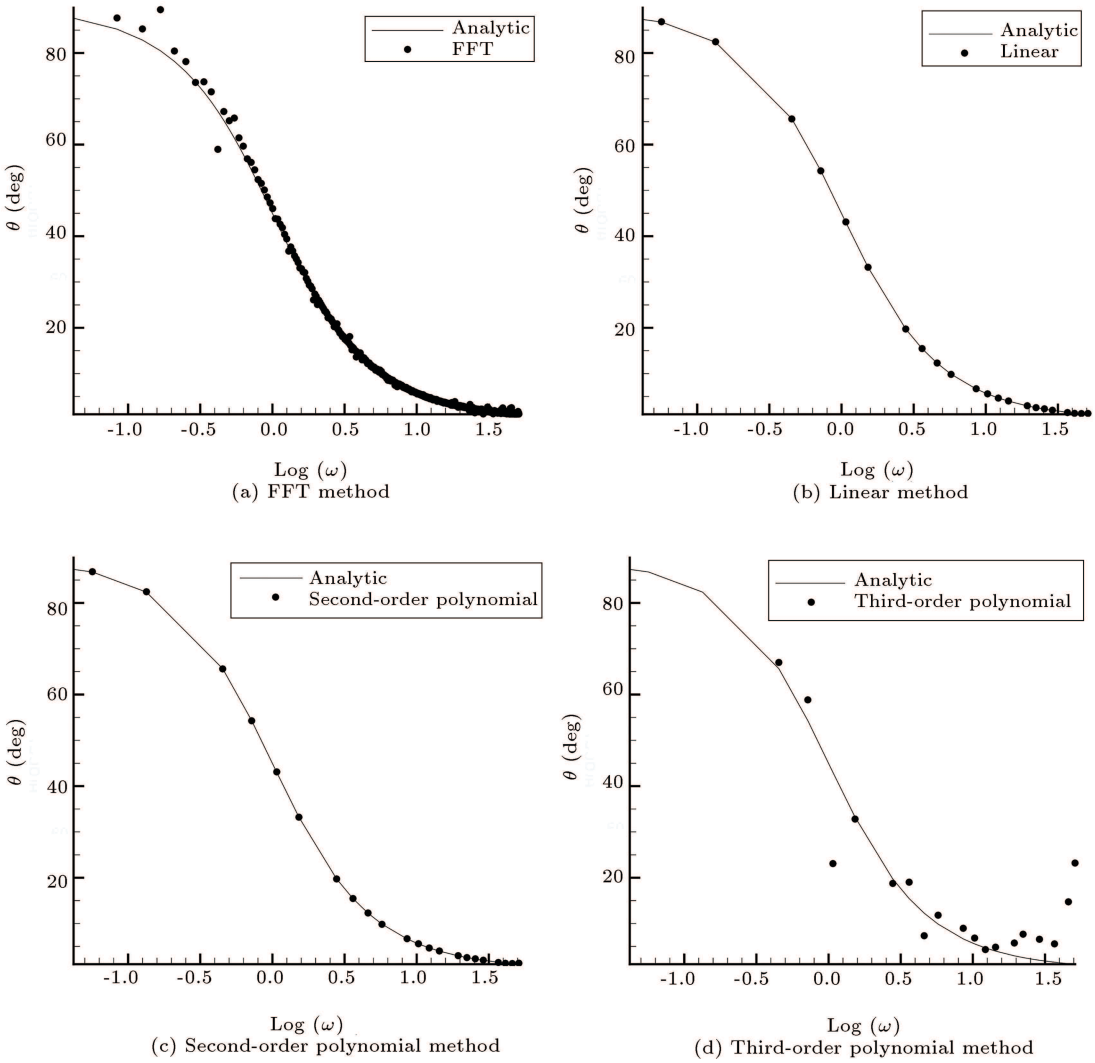

Figure 7. Impedance phase plot of the series circuit in the condition described in Table 2.

lower than those of the FFT, second-order polynomial, and third-order polynomial methods. Therefore, it can be concluded that increasing the solution order of the FT from zero up to one can improve the responses. More increase (greater than one), however, proved to deteriorate the responses.

The Nyquist diagrams of the parallel circuit impedance (according to Table 2) calculated from the FFT, linear, second-order polynomial, and third-order polynomial methods are demonstrated in Figure 8(a)–(d), respectively. Of note, sharper oscillations are observed in the diagram of the FFT method than that observed in the analytical impedance Nyquist diagram. All in all, the linear method is in good agreement with the analytical Nyquist plot. Moreover, the second-order and third-order polynomial methods considerably differ from the analytical mode (no semicircle form); hence, no correct responses were obtained. In this regard, despite the fact that increasing the solution order of the FT from zero up to one would yield good results, further increase would no longer improve responses and instead, it would deteriorate them.

The parallel circuit impedance magnitude diagrams with respect to the frequency (the bode plot) calculated from the FFT, linear, second-order polynomial, and third-order polynomial methods are depicted in Figure 9(a)–(d), respectively. The impedance phase diagrams of the parallel circuit (bode plot) calculated through the FFT, linear, second-order polynomial, and third-order polynomial methods are also demonstrated in Figure 10(a)–(d), respectively. A similar outcome to the Nyquist impedance diagrams can be detected in the mentioned diagrams (impedance magnitude and phase bode plots). Additionally, there are some parts with high oscillations in the corresponding diagram of the FFT method. However, the linear method shares a significant resemblance with the analytical method. It should also be mentioned that the second- and third-order polynomial methods did not yield a correct response at all. The results obtained from

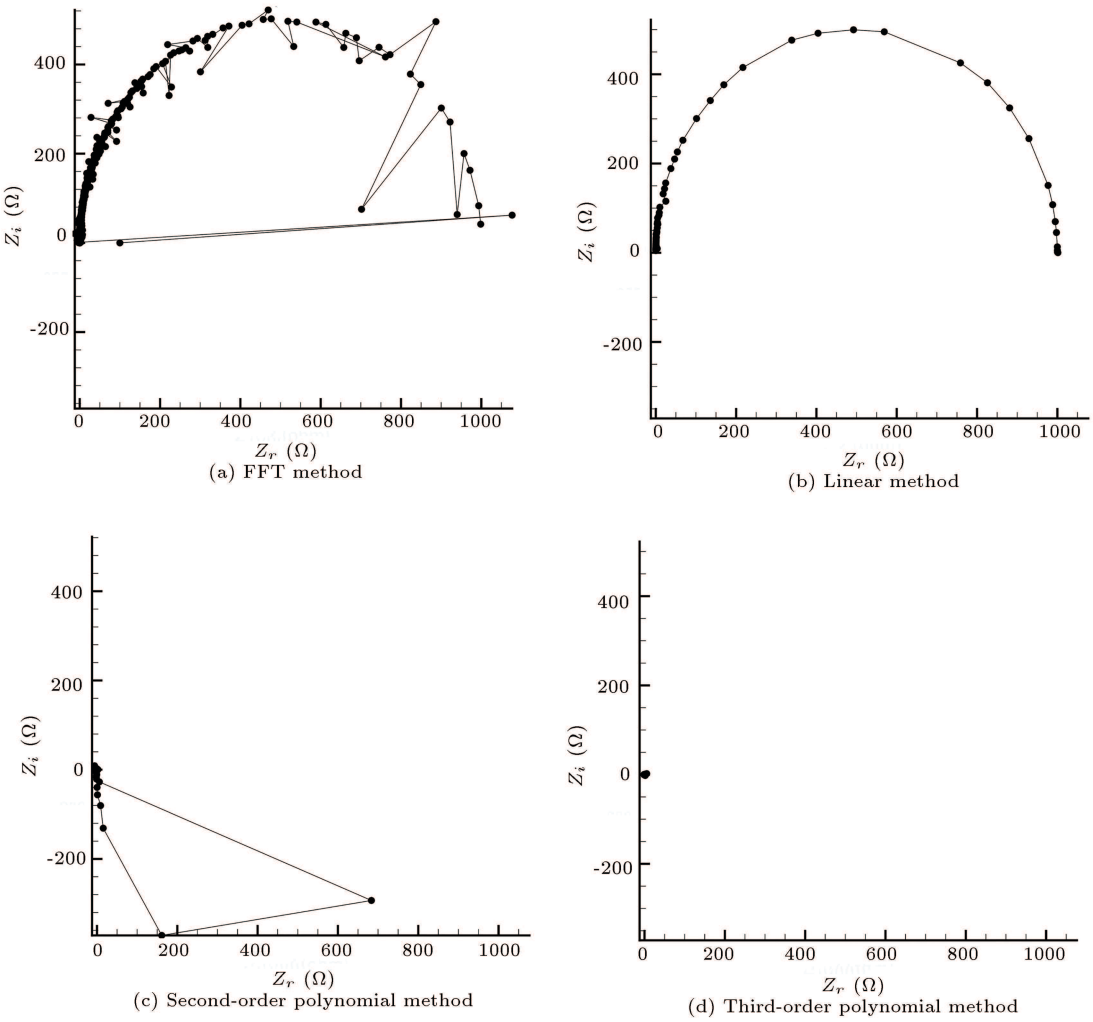

Figure 8. Impedance Nyquist plot of the parallel circuit in the condition described in Table 2.

Table 4. The errors in the parallel circuit.

Error type	FFT	Linear	Second-order	Third-order
Δ_{re}	1.6180	0.0140	0.3045	0.2401
Δ_{im}	7.8625	0.0169	0.8588	0.8589
s	3.3725×10^7	0.2441	8.3841×10^6	2.3467×10^{14}

the error measurement are presented in Table 4. As perceived, the linear method shows less error than all other methods; hence, it can be concluded that it is the most appropriate technique among the investigated methods. As mentioned earlier, increasing the solution order from one to higher orders deteriorates the acquired responses.

3.2. Battery circuit

In the EIS method, various models are considered to be implemented in the Li-ion batteries. One of the most famous models is the second-order Thevenin topology, which is demonstrated in Figure 11. In this figure, R_1, R_2, and R_0 represent the ohmic resistance, and C_1 and C_2 indicate the capacitor. Numerous studies have considered the application of model in the Li-ion batteries [28–31]. A parallel resistor and capacitor define the order of each circuit. According to this definition, the circuit shown in Figure 11 is a second-order type since it has two pairs of parallel capacitor and resistor. As the order of circuits increases, the model becomes more real; however, such increase enhances the model complexity. In many cases, the resulting complexity is significantly greater than the required accuracy. For this reason, making a balance and achieving an optimum state between the complexity and accuracy

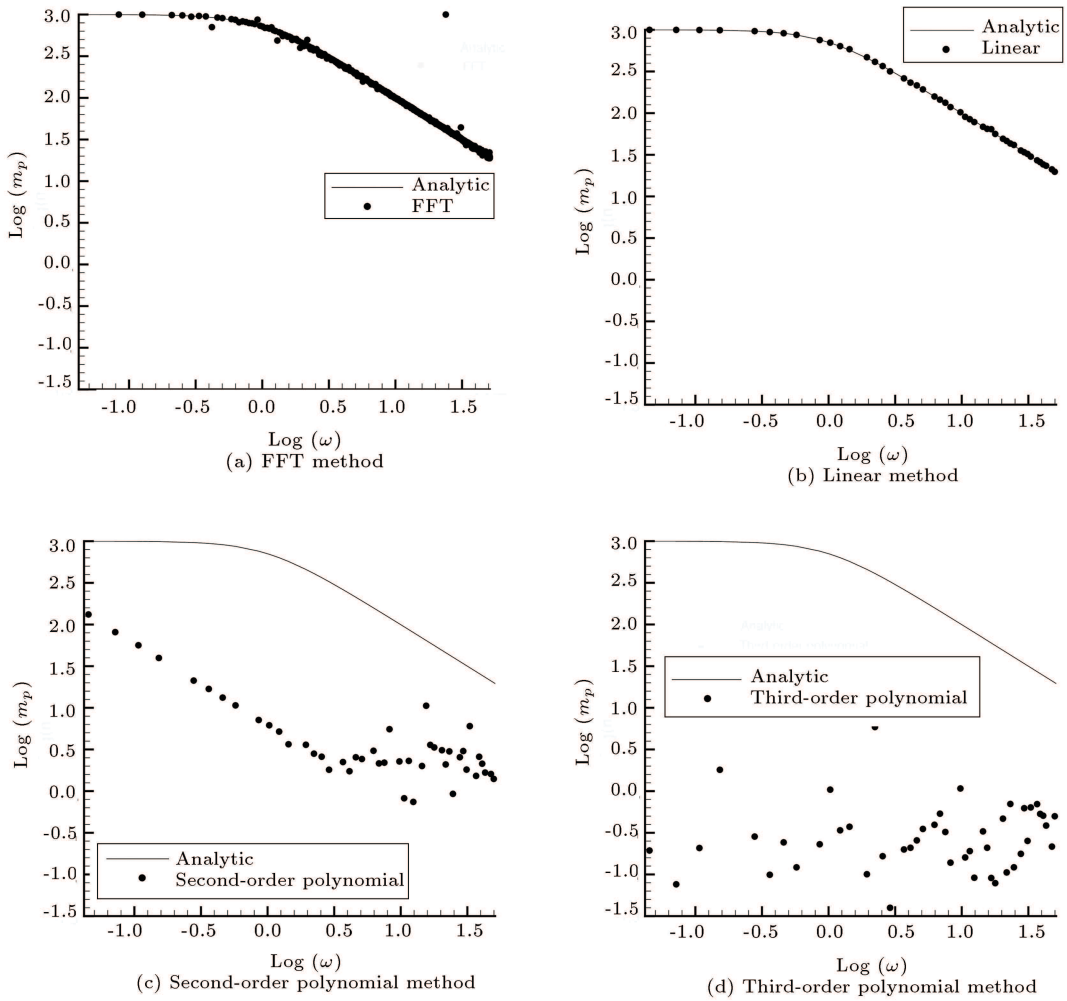

Figure 9. Impedance magnitude plot of the parallel circuit in the condition described in Table 2.

seem necessary. In such cases, second- and third-order models are often employed [32,33]. Numerous studies verified that the second-order Thevenin circuit was the best circuit for the Li-ion battery. To be specific, [34] investigated this finding and confirmed that this circuit would be a good candidate circuit for the Li-ion battery.

The impedance of the equivalent circuit presented in Figure 11 can be calculated using Eq. (21). In this equation, Z_B is the impedance of the battery equivalent circuit, and ω is the frequency.

$$Z_B = \frac{R_1}{1 + jR_1C_1\omega} + \frac{R_2}{1 + jR_2C_2\omega} + R_0. \tag{21}$$

The battery model is developed based on Figure 11, and the parameters of this model are determined according to Table 5. The data presented in Table 5 resemble that given in Ref. [31] that were obtained for the NMC Li-ion battery at SoC=1 under real circumstances. By substituting the parameters of Table 5 into Eq. (21), the analytical impedance of the battery model can be achieved in actual circumstances. Next, the battery model (Figure 11) is simulated in Scilab software according to Table 2 (except for the resistance and capacitance values) to obtain the system response. Subsequently, the battery model impedance is calculated by FFT, linear, and second- and third-order polynomial FT of voltage and current. Finally, the calculated impedances are compared with the analytical impedance, as discussed in the previous section.

The Nyquist diagram of the battery model impedance calculated by the FFT, linear as well as the second- and third-order polynomial methods are demonstrated in Figure 12(a)–(d). Some outliers accompanied by sharp oscillations are observed in the corresponding diagram of the FFT method. However, the points here are similar to those of the analytical method in the linear method diagram. Moreover, in the second-order polynomial method, the general form of the diagram resembles the analytical mode; however, the distances between the points in the analytical method are longer than those in the linear method. In the third-order polynomial technique, there are

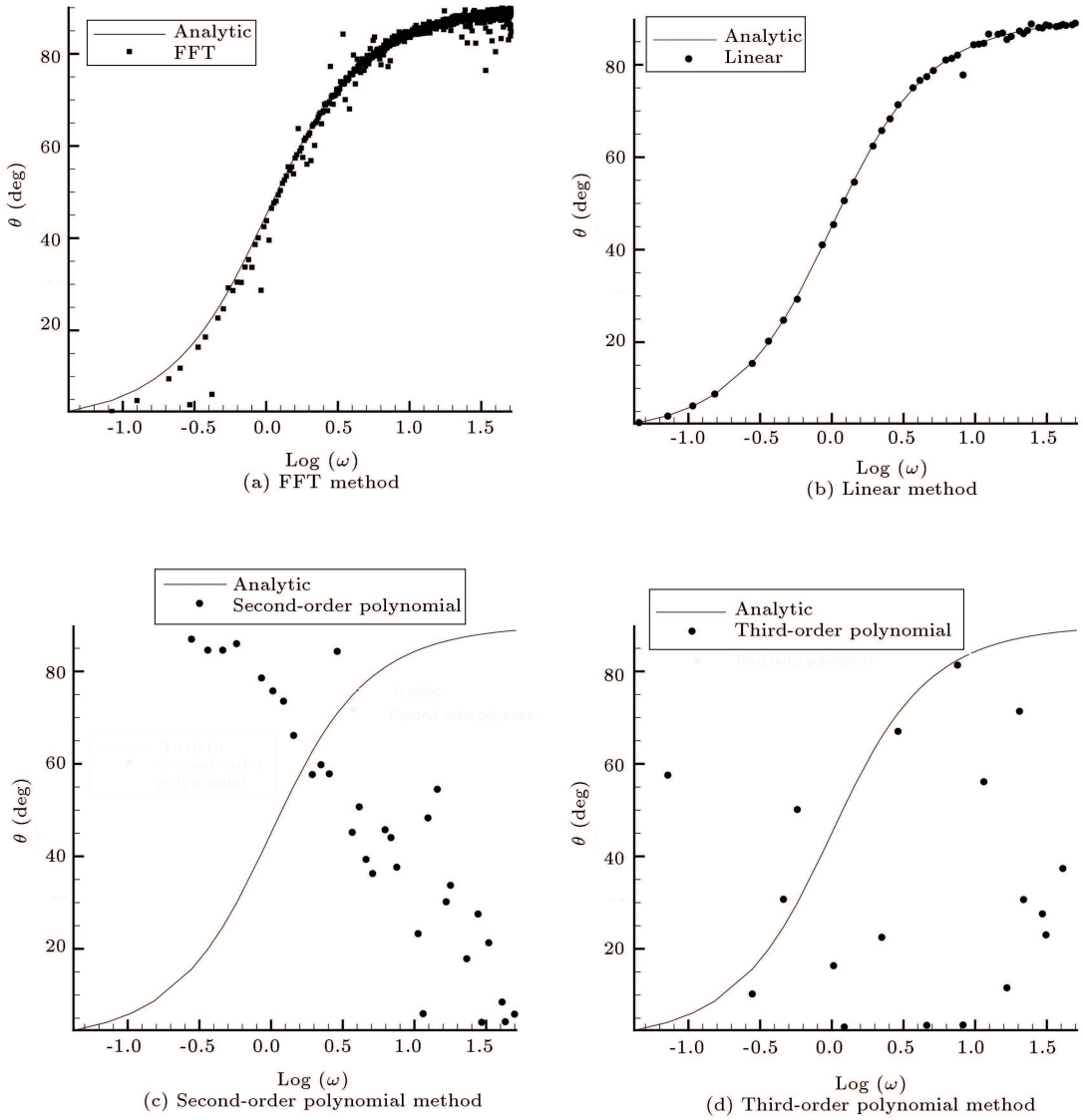

Figure 10. Impedance phase plot of the parallel circuit in the condition described in Table 2.

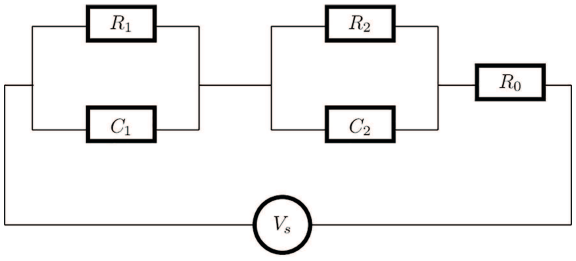

Figure 11. Battery model in according to second-order or Thevenin circuit model.

extreme outlier points that cannot ensure appropriate responses. Therefore, in its corresponding diagram (Figure 12(d)), the values of the lower and upper bounds of the horizontal and vertical axes of the diagram are not similar to those in the other three Figure 12(a)–(c).

The diagram of the battery model impedance magnitude with respect to the frequency (the bode plot) calculated by the FFT, linear, and second- and third-order polynomial methods are illustrated in Figure 13(a)–(d), respectively. As perceived, similar to the previous sections, sharp oscillations are observed in the corresponding diagram of the FFT method. However, the linear method share significant resemblance with the analytical method. In addition, the second-order polynomial method is in good agreement with the analytical method. However, no correspondence exists between the corresponding diagrams of the simulated data of the third-order polynomial and analytical methods. It must be mentioned that identical to the previous paragraph, the upper and lower bounds of the vertical axis of Figure 13(d) are not similar to those of other diagrams for better demonstration of all obtained data of the third-order polynomial.

The diagram of the battery model impedance

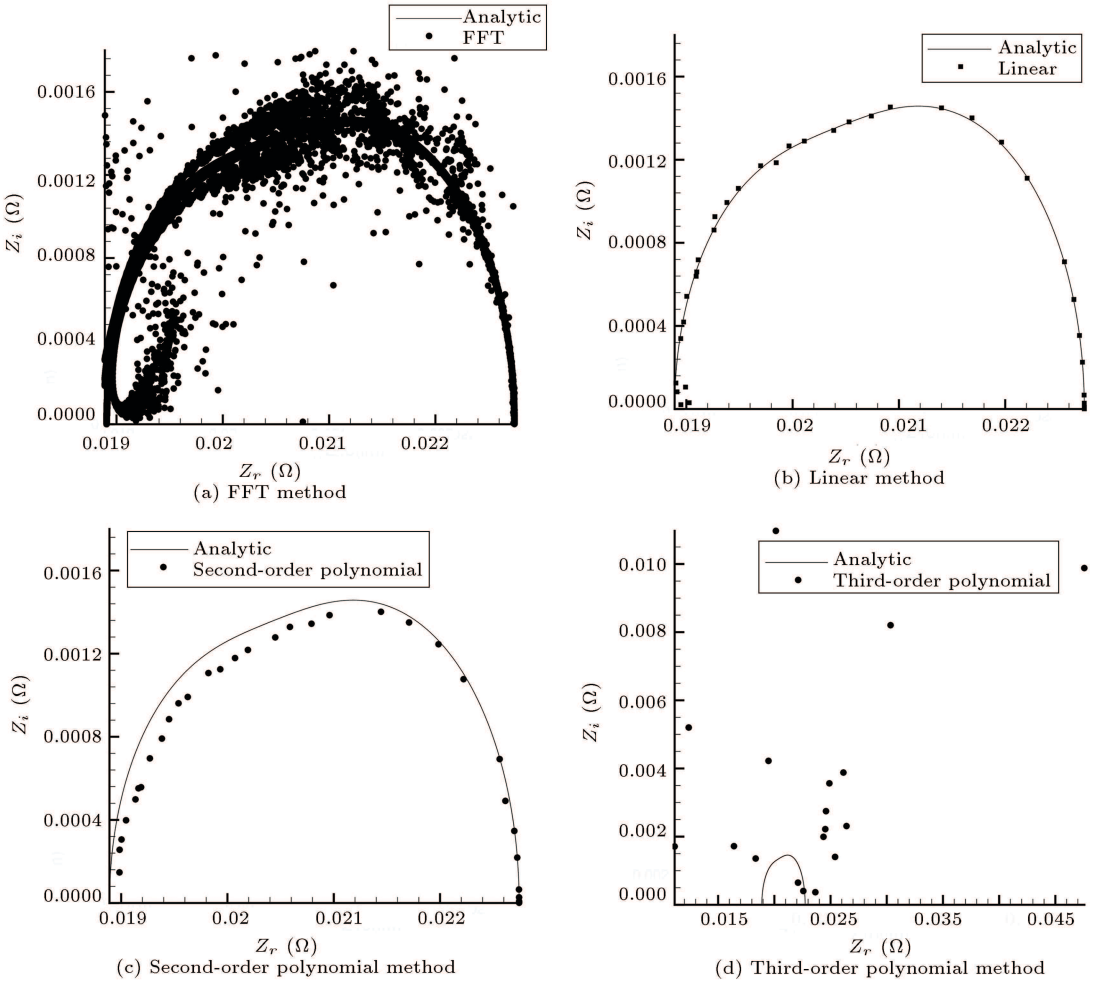

Figure 12. Impedance Nyquist plot of the battery model in the condition described in Tables 2 and 5.

Table 5. The actual value of the NMC li-ion battery parameters [31].

SoC	V_s (v)	$R_0(\Omega)$	R_1 (Ω)	C_1 (F)	R_2 (Ω)	C_2 (F)
1	4.195754	0.01889	0.001540	1.241	0.002314	4.626

phase with respect to the frequency (the bode plot) calculated using the FFT, linear, second-order polynomial, and third-order polynomial methods are depicted in Figure 14(a)–(d), respectively. Accordingly, high oscillations are evident in the corresponding diagram of the FFT method. However, similar to the previous sections, there is excellent agreement between the simulated data of the linear method and the analytical diagram. Moreover, there is a good resemblance between the corresponding diagrams of the second-order polynomial method data and analytical method diagram; nevertheless, this resemblance is less than that of the linear method. In the third-order polynomial method, there is no similarity between the analytical diagram and simulated data (the obtained simulation data are outliers). Therefore, the vertical axis of Figure 14(d) is entirely different from that of other diagrams to better represent data.

The obtained results from error calculation are presented in Table 6 according to which, the linear method has less error rate than all other methods, hence the most appropriate technique among the examined methods. Similar to the previous section, increasing the solution order to the second- and third-order does not yield good results and instead, it deteriorates the acquired responses.

4. Conclusion

In the present research, the effect of higher-order integration on the simulation of Fourier Transform (FT) for

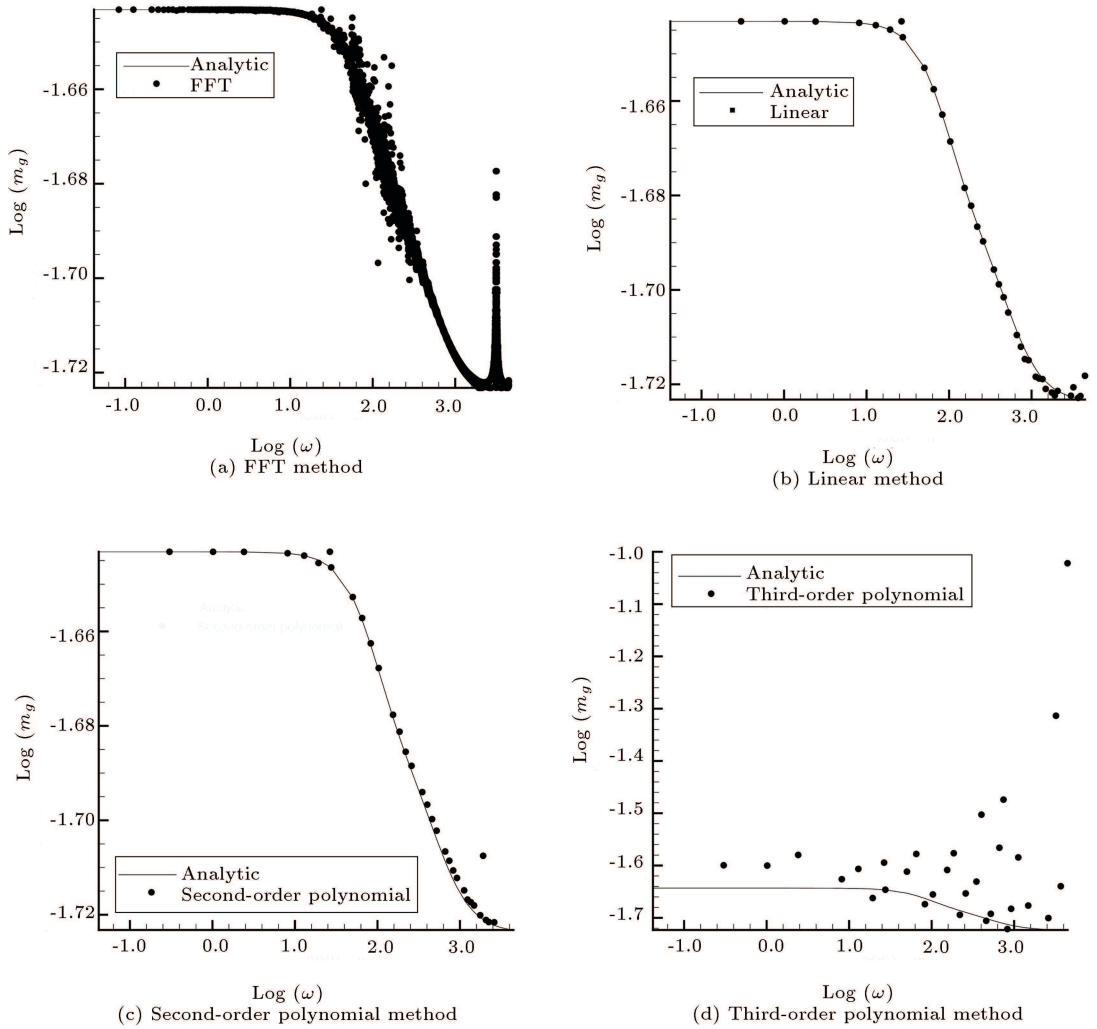

Figure 13. Impedance magnitude plot of the battery model in the condition described in Tables 2 and 5.

Table 6. The errors in the battery model.

Error type	FFT	Linear	Second-order	Third-order
Δ_{re}	0.129	0.0016	0.0060	0.2872
Δ_{im}	0.0249	0.0057	0.0103	0.2730
s	278.1929	0.0044	0.0541	5.1271

discrete data was investigated. The main inspiration behind this study originated from the failure of the conventional Fast Fourier Transform (FFT) method in obtaining accurate results when applied to noisy data, the case in the experimental tests. To investigate the effects of higher-order integration, first-, second-, and third- order polynomial methods were compared to calculate the numerical FT of both voltage and current. These methods were then applied to obtain the impedance spectra of three different circuits namely (a) a capacitor and resistor in series, (b) a capacitor and resistor in parallel, and (c) a conventional battery circuit model. All the series were triggered by a noisy step-wise signal. The obtained results were then compared with those from the FFT method. It was expected that increasing the FT solution order would improve the responses. The findings revealed that although moving from zero- to first-order polynomial enhanced the method robustness, further increase led to a negative outcome. In other words, increasing the solution order of the integration did not necessarily improve the responses. Ultimately, it was concluded that the most appropriate method for the electrochemical impedance spectroscopy in the time domain under

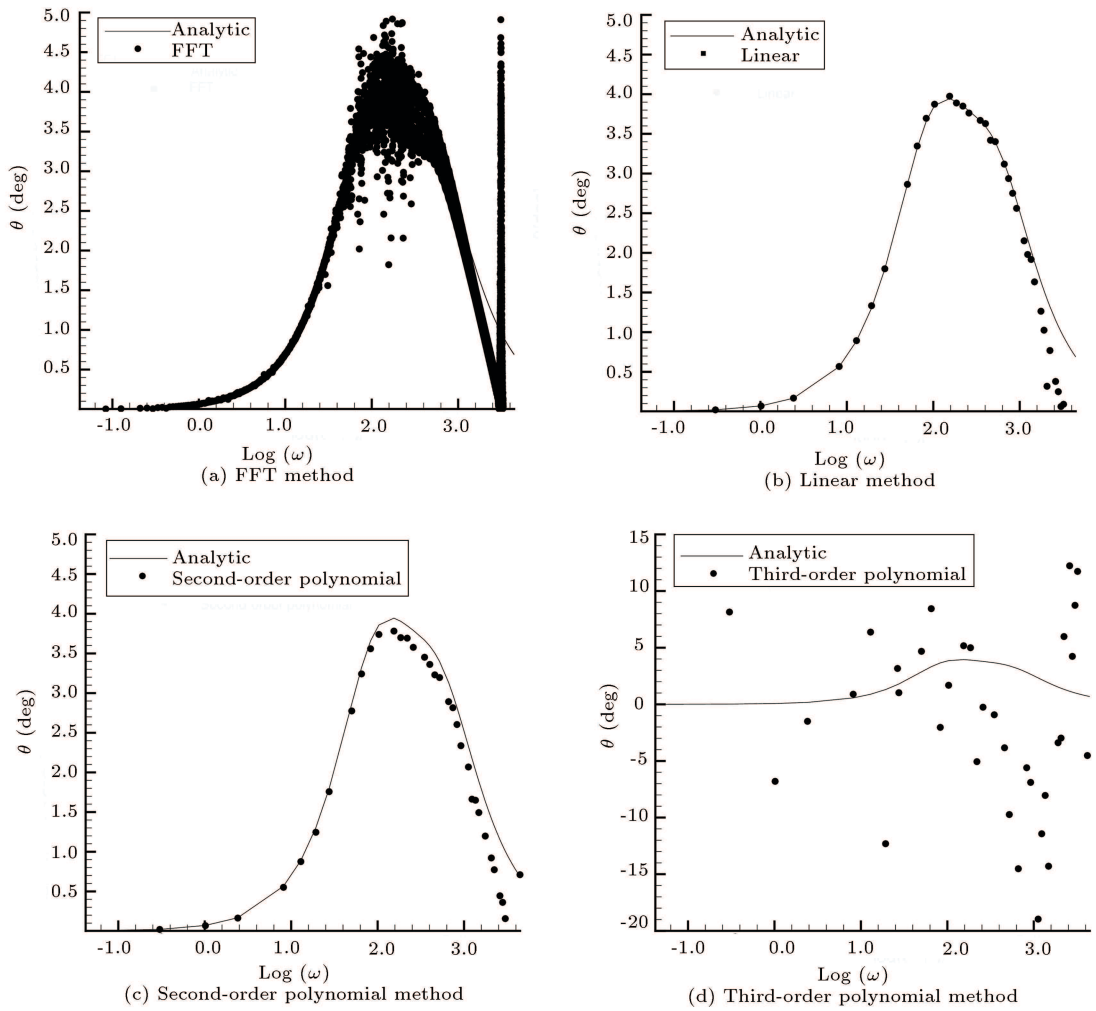

Figure 14. Impedance phase plot of the battery model in the condition described in Tables 2 and 5.

noisy conditions was the linear method that also helped calculate the FT of both current and voltage.

Abbreviations

EIS	Electrochemical Impedance Spectroscopy
FFT	Fast Fourier Transform
FT	Fourier Transform
Li	Lithium
$Li-S$	Lithium sulfur
NMC	Nickel Manganese Cobalt
SoC	State of Charge
SoH	State of Health

Nomenclature

$a_0, ..., a_{m-1}, a_m$	Constant coefficients of the mth-order polynomial of voltage between t_{nm+1} and $t_{(n+1)m+1}$
C	Capacitance, F
C_1	Capacitance of the negative electrode, F
C_2	Capacitance of the positive electrode, F
F_k	Discrete Fourier transform of the function f at k frequency
f_i	Value of the function f at the ith point
$f(t)$	Arbitrary function
$f(\omega)$	Fourier transform of arbitrary function $f(t)$
I	Current, A
$I(\omega)$	Fourier transform of current
$Im_I(\omega)$	Imaginary part of current Fourier transform
$Im_V(\omega)$	Imaginary part of voltage Fourier transform
i	Counter of the number of points
m	Degree of polynomial
m_p	Impedance magnitude of parallel circuit, Ω

m_s	Impedance magnitude of series circuit, Ω
N_g	Number of mth-order polynomials
R	Resistance, Ω
R_0	Electrolyte resistance, Ω
R_1	Resistance of negative electrode, Ω
R_2	Resistance of positive electrode, Ω
$Re_I(\omega)$	Real part of current Fourier transform
$Re_V(\omega)$	Real part of voltage Fourier transform
s	Object function, the criterion for calculation of error
t	Time, s
t_{nm+1}	Beginnig time of integration, s
$t_{(n+1)m+1}$	End time of integration, s
V	Voltage, v
$v_0, \cdots, v_{m-1}, v_m$	Corresponding voltages of each $m+1$ successive points of t_0,$\cdots$,t_{m-1},t_m, v
$V(\omega)$	Fourier transform of voltage
w_i	Inverse of the square of the vector length of impedance in ith frequency
$Z(\omega)$	Impedance, Ω
Z_B	Battery model impedance, Ω
$Z_{a,i}$	Analytical impedance in ith frequency, Ω
$Z_{im,i}$	Measured imaginary part of impedance in ith frequency, Ω
$Z_{ima,i}$	Analytical imaginary part of impedance in ith frequency, Ω
Z_p	Parallel circuit impedance, Ω
$Z_{p,re}$	Real part of parallel circuit impedance, Ω
$Z_{p,im}$	Imaginary part of parallel circuit impedance, Ω
$Z_{re,i}$	Measured real part of impedance in ith frequency, Ω
$Z_{rea,i}$	Aanalytical real part of impedance in ith frequency, Ω
Z_s	Series circuit impedance, Ω
$Z_{s,re}$	Real part of series circuit impedance, Ω
$Z_{s,im}$	Imaginary part of series circuit impedance, Ω

Greek

Δ_{im}	Mean relative error of imaginary part of impedance
Δ_{re}	Mean relative error of real part of impedance
ω	Frequency, Hz
θ	Phase, deg
θ_p	Impedance phase of parallel circuit, deg
θ_s	Impedance phase of series circuit, deg

References

1. Janicka, E., Mielniczek, M., Gawel, L., et al. "The impact of air humidity on the operation of proton exchange membrane fuel cells determined using dynamic electrochemical impedance spectroscopy", *Electrochimica Acta*, **341**, 136036 (2020).
2. Qiu, X., Hua, Q., Zheng, L., et al. "Study of the discharge/charge process of lithium-sulfur batteries by electrochemical impedance spec-troscopy", *RSC Advances*, **10**(9), pp. 5283–5293 (2020).
3. Sharma, D.K., Pareek, K., and Chowdhury, A. "Investigation of solar cell degradation using electrochemical impedance spectroscopy", *International Journal of Energy Research*, **44**(11), pp. 8730–8739 (2020).
4. Xiao, H., Tao, Z., Bai, H., et al. "State of charge effects on the parameters of electrochemical impedance spectroscopy equivalent circuit model for lithium ion batteries", In *IOP Conference Series: Earth and Environmental Science*, **474**(5), IOP Publishing, 052038 (2020).
5. Gallo, M., Polverino, P., Mougin, J., et al. "Coupling electrochemical impedance spectroscopy and model-based aging estimation for solid oxide fuel cell stacks lifetime prediction", *Applied Energy*, **279**, 115718 (2020).
6. Erts, D., Katkevics, J., Sjomkane, M., et al. "Eis characterization of aging and humidity-related behavior of bi2se3 films of different morphologies", *Nano-Structures and Nano-Objects*, **30**, 100847 (2022).
7. Calles, S. Heitjans, P., and Börger, A. "Electrochemical impedance spectroscopic studies of phev2 form-factor lithium-ion cells for automotive applications", *Journal of Energy and Power Technology*, **4**(2), pp. 1–28 (2022).
8. Gopalakrishnan, R., Li, Y., Smekens, J., et al. "Electrochemical impedance spectroscopy characterization and parameterization of lithium nickel manganese cobalt oxide pouch cells: dependency analysis of temperature and state of charge", *Ionics*, **25**(1), pp. 111–123 (2019).
9. Li, D., Yang, D., Li, L., et al. "Electrochemical impedance spectroscopy based on the state of health estimation for lithium-ion batteries", *Energies*, **15**(18), 6665 (2022).
10. Koseoglou, M., Tsioumas, E., Ferentinou, D., et al. "Lithium plating detection using dynamic electrochemical impedance spectroscopy in lithiumion batteries", *Journal of Power Sources*, **512**, 230508 (2021).
11. Ezpeleta, I., Freire, L., Mateo-Mateo, C., et al. "Characterisation of commercial liion batteries using electrochemical impedance spectroscopy", *ChemistrySelect*, **7**(10), e202104464 (2022).

12. Capkova, D., Knap, V., Fedorkova, A.S., et al. "Analysis of 3.4 ah lithium-sulfur pouch cells by electrochemical impedance spectroscopy", *Journal of Energy Chemistry*, **72**, pp. 318–325 (2022).

13. Mohsin, M., Picot, A., and Maussion, P. "A new lead-acid battery state-of-health evaluation method using electrochemical impedance spectroscopy for second life in rural electrification systems", *Journal of Energy Storage*, **52**, 104647 (2022).

14. Lohmann, N., Weßkamp, P., Haußmann, P., et al. "Electrochemical impedance spectroscopy for lithium-ion cells: Test equipment and procedures for aging and fast characterization in time and frequency domain", *Journal of Power Sources*, **273**, pp. 613–623 (2015).

15. Klotz, D., *Characterization and Modeling of Electrochemical Energy Conversion Systems by Impedance Techniques*, KIT Scientific Publishing (2014).

16. Gantenbein, S., Weiss, M., and Ivers-Tiffée, E. "Impedance based time-domain modeling of lithium-ion batteries: Part *i*", *Journal of Power Sources*, **379**, pp. 317–327 (2018).

17. Jiang, Z., Yao, J., Wang, L., et al. "Development of a portable electrochemical impedance spectroscopy system for bio-detection", *IEEE Sensors Journal*, **19**(15), pp. 5979–5987 (2019).

18. Lyu, C., Zhang, T., Luo, W., et al. "Soh estimation of lithium-ion bat- teries based on fast time domain impedance spectroscopy", In *2019 14th IEEE Conference on Industrial Electronics and Applications (ICIEA)*, IEEE, pp. 2142–2147 (2019).

19. Lyu, C., Liu, H., Luo, W., et al. "A fast time domain measuring technique of electrochemical impedance spectroscopy based on fft", In *2018 Prognostics and System Health Management Conference (PHM-Chongqing)*, IEEE, pp. 450–455 (2018).

20. Zappen, H., Ringbeck, F., and Sauer, D.U. "Application of time-resolved multi-sine impedance spectroscopy for lithiumion battery characterization", *Batteries*, **4**(4), p. 64 (2018).

21. Kuznietsov, A., Happek, T., and Kiselev, A. "Onboard impedance spectroscopy of lithium-ion batteries in electrical vehicles: Comparative analysis of injected signals and practical implementation", In *ELECTRIMACS 2019*, Springer, pp. 75–88 (2020).

22. De Angelis, A., Buchicchio, E., Santoni, F., et al. "Uncertainty characterization of a practical system for broadband measurement of battery EIS", *IEEE Transactions on Instrumentation and Measurement*, **71**, pp. 1–9 (2022).

23. Fu, Y., Xu, J., Shi, M., et al. "A fast impedance calculation based battery state-of-health estimation method", *IEEE Transactions on Industrial Electronics*, **69**(7), pp. 7019–7028 (2021).

24. Alavi, S., Birkl, C., and Howey, D. "Time-domain fitting of battery elec-trochemical impedance models", *Journal of Power Sources*, **288**, pp. 345–352 (2015).

25. Bullecks, B., Suresh, R., and Rengaswamy, R. "Rapid impedance measurement using chirp signals for electrochemical system analysis", *Computers and Chemical Engineering*, **106**, pp. 421–436 (2017).

26. Klotz, D., Schönleber, M., Schmidt, J., et al. "New approach for the calculation of impedance spectra out of time domain data", *Electrochimica Acta*, **56**(24), pp. 8763–8769 (2011).

27. Yuan, X.-Z., Song, C., Wang, H., et al. *Electrochemical Impedance Spectroscopy in PEM Fuel Cells: Fundamentals and Applications*, Springer Science and Business Media (2009).

28. Nikolian, A., Jaguemont, J., De Hoog, J., et al. "Complete cell-level lithium-ion electrical ECM model for different chemistries (NMC, IFP, ITO) and temperatures (- 5°C to 45°C)–optimized modelling techniques", *In- ternational Journal of Electrical Power and Energy Systems*, **98**, pp. 133–146 (2018).

29. Gong, X. "Modeling of lithium-ion battery considering temperature and aging uncertainties", PhD dissertation (2016).

30. Madani, S.S., Schaltz, E., and Knudsen Kær, S., "An electrical equivalent circuit model of a lithium titanate oxide battery", *Batteries*, **5**(1), p. 31 (2019).

31. Vyroubal, P. and Kazda, T. "Equivalent circuit model parameters extraction for lithium ion batteries using electrochemical impedance spectroscopy", *Journal of Energy Storage*, **15**, pp. 23–31 (2018).

32. Leinonen, J. "Real-time electrical emulation of li-ion battery storage using power-hardware-in-the-loop", Master's Thesis (2019).

33. Huria, T., Ceraolo, M., Gazzarri, J., et al. "High fidelity electrical model with thermal dependence for characterization and simulation of high power lithium battery cells", In *2012 IEEE International Electric Vehicle Conference*, IEEE, pp. 1–8 (2012).

34. Tran, M.-K., DaCosta, A., Mevawalla, A., et al. "Comparative study of equivalent circuit models performance in four common lithium-ion batteries: LFP, NMC, IMO, NCA", *Batteries*, **7**(3), p. 51 (2021).

Biographies

Razieh Hamedi is a PhD student at K.N. Toosi University of technology, Faculty of Mechanical Engineering, Tehran, Iran. Her main research interest is renewable energies.

Farschad Torabi is an Associate Professor of Mechanical Engineering at K.N. Toosi University of Technology, Iran. His research interests include renewable energies, batteries, and electrochemical systems. His major research studies primarily focus on the numerical

simulation as well as application of a combination of computational fluid mechanics and analytical methods.

Jahan Bakhsh Ghasemi is a Professor in the Chemistry Department, Faculty of Sciences, University of Tehran, Iran. His earned his PhD degree in Analytical Chemistry and conducted several research studies on the thermodynamic and kinetic of complexation. His main research interests are the thermodynamic and kinetic study of ligands, microfluidic, software applications for analytical data refinement, interfacing, automation, and application of different chemometrics techniques. He authored five books, published 250 papers in international journals, and attended in more than 200 conferences.